Analytic Bound on Accuracy of Battery State and Parameter Estimation

Xinfan Lin[z] and Anna G. Stefanopoulou

Department of Mechanical Engineering, University of Michigan, Ann Arbor, Michigan 48109, USA

Methods for battery state and parameter estimation have been widely investigated, while the achievable accuracy of the estimation remains a critical but somehow overlooked topic. In this paper, the analytic bounds on the accuracy of battery state and parameter estimation accounting for voltage measurement noises are derived based on the Fisher information matrix and Cramer-Rao bound analysis. The state and parameters under discussion include the state of charge, capacity and (ohmic) resistance. The estimation accuracy is influenced by the information contained in the data set used for estimation. It is found that the main contributing factors to the accuracy of SOC estimation are the slope of the OCV curve and number of data points, while the accuracy of capacity estimation is affected by both OCV slope and SOC variation, and that of resistance estimation depends heavily on the current magnitude. The analytic bounds are derived for both standalone estimation, where only one state/parameter is estimated, and combined estimation where they are estimated together. The loss of accuracy in combined estimation compared to standalone estimation is usually expected. However, when the current excitation satisfies certain patterns, such loss can be avoided. The conclusions can be used as guidelines for offline experiment design as well as online evaluation of the accuracy of adaptive state and parameter estimation.

Battery state and parameter estimation has been studied extensively in literature. Critical battery states include state of charge (SOC), temperature, state of power (SOP) and state of health (SOH) among others. As for the parameters, some of them are commonly seen in almost all types of models, such as the (ohmic) internal resistance, capacity, and open circuit voltage (OCV). Others are model-specific, especially those relating to the transient battery dynamics, e.g. R-C circuits in the equivalent circuit model, or diffusion coefficient/electrical conductivity in the electrochemical model. In this paper, the discussion will be limited to SOC, resistance and capacity, but the methodology can be extended to other states and parameters. It is noted that state estimation and parameter estimation are greatly interconnected for two reasons. For one thing, some of the states are in fact defined based on certain parameters. For example, it is well known that as battery ages, its capacity decreases[1–3] while resistance grows.[4–6] Therefore, SOH is often defined as the ratio of the remaining capacity and the nominal capacity, or the ratio of the actual (degraded) resistance and the nominal resistance.[7] For another, it has been shown that the accuracy of state estimation will be greatly affected by the precision of parameters.[8]

Various methods have been proposed in literature for battery state and parameter estimation. For SOC estimation, the basic method is coulomb counting,[9–10] where the current is integrated over time to calculate the change in stored energy. Since this method is susceptible to inaccurate initial SOC and current measurement bias/noise, corrections based on OCV under rest is often applied to improve estimation accuracy.[11] When the battery is under load, however, due to the unavailability of OCV, model-based methods are typically used, which combine model, and current and voltage measurement. The commonly used models include the OCV-R model,[9] equivalent circuit model,[12–13] neural network model,[16,17] electrochemical models[18,19] and the simplified versions[20–23] among others. As for the estimation algorithm, the most widely used one is the extended Kalman filtering (EKF) originally reported in Ref. 24. Others include but are not limited to unscented Kalman filtering (UKF),[25] sliding mode observer,[26] H_∞ observer,[27] and Partial Differential Equation (PDE)-based observer.[28] The topic has also been studied under reduced voltage sensing, where only the total voltage of two (or more) cells connected in series is measured.[29,30] Nonlinear observers, such as the Newton observer and sliding mode observer, are designed to solve the SOC estimation problem. As for battery capacity and resistance estimation, it can be performed separately from SOC estimation, and the explored methods in literature include least-squares based algorithm,[31,32] particle filtering,[33]

Lyapunov-based adaptation[34] among others. There have also seen substantial efforts addressing combined estimation of SOC and capacity/resistance, mostly based on EKF. For example, dual extended Kalman filtering (DEKF)[35] has been used to estimate the battery SOC and capacity/resistance in a sequential way, which further includes the synchronized (standard) DEKF[36–38] and the multi-time-scale DEFK where the SOC and capacity are updated at different rates.[39,40] Joint extended Kalman filter (JEKF) has also been studied, which updates the SOC and capacity estimation simultaneously.[41,42]

Another important aspect of the estimation problem, the achievable accuracy of estimation from available data, has not been equally emphasized in the previous study though. Related topics include analysis on sensitivity, confidence interval and error bound among others. There have seen increasing interests in the field recently. In Ref. 43, the sensitivity of the output voltage to the parameters of an electrochemical model is quantified based on simulation under parameter perturbation. Similarly, in Ref. 44, the sensitivity of capacity estimation is studied by calculating the deviation of estimates under perturbation of other parameters. In Ref. 45, the confidence interval of parameter estimation is obtained through Monte Carlos simulation. Other works are mainly based on Fisher information analysis,[46] which measures the sufficiency of data for state/parameter estimation. For example, in Ref. 47 the eigenvalues of the Fisher information matrix are used to determine and group the strongly identifiable parameters. In Ref. 48, the Fisher-Information-based Cramer-Rao bounds, which quantifies the theoretical lower bound of the variance of estimates, are numerically calculated for parameters of an electrochemical battery model. In Ref. 49, the confidence intervals of the estimates are obtained based on Analysis of Variance (ANOVA). In Refs. 50 and 51, the relationship between the estimation accuracy and the characteristics of the data set, such as the SOC range, number of data points and current magnitude, is studied based on Cramer-Rao bound analysis. The expression of the Fisher information matrix of the OCV-R model under periodic current excitation is also derived in Ref. 50. In Ref. 52, the attempt is made to enhance the identifiability by choosing the current excitation that maximizes the determinant of the Fisher information matrix.

In this paper, the analytic bounds on estimation accuracy of SOC, capacity and resistance will be derived under various circumstances. The unique contributions of the paper include the following three aspects. First, the lower bound of the variance of the estimation is analytically derived based on the equivalent circuit model, which shows the contributing factors to estimation accuracy in an explicit way. Most of the existing works focus on computing the numerical bounds. Second, the analytic bound is studied for standalone estimation as well as combined state and parameter estimation. Standalone estimation refers to

[z]E-mail: xflin@umich.edu

the case that only one state or parameter is being estimated, assuming all others are known, e.g. estimating SOC based on known capacity. In reality, however, multiple states and/or parameters may need to be estimated. For example, battery capacity degrades over lifetime,[1–3] making the SOC estimation based on the nominal capacity inaccurate. Estimation of multiple state/parameters, which includes both the dual estimation and joint estimation as mentioned in the literature review, is referred to as combined estimation here. The accuracy of combined estimation will usually deteriorate as compared to that of standalone estimation. The loss of accuracy is quantified through comparison in this paper. More importantly, it is also found that the loss of accuracy can be avoided when the current input is designed to satisfy certain patterns, which enlightens the experiment design. Third, the analytic bound will be evaluated under some commonly used/seen current inputs, such as the constant and square-wave currents, revealing practical and easily perceptible insights. The conclusions can be used as guidelines for designing offline experiments for identification as well as evaluating the accuracy of online state/parameter estimation. The analysis is conducted based on control-oriented battery electrical models, but it could provide insight for generic battery models.

Methodology: Fisher Information Matrix and Cramer-Rao Bound

The basics about the Fisher information matrix and the Cramer-Rao bound are introduced in this section. Consider the following nonlinear discrete-time plant model,

$$x_{k+1} = f(x_k, \theta_k, u_k), \quad x \in \mathbf{R}^n, \theta \in \mathbf{R}^m, u \in \mathbf{R}$$

$$y_k = h(x_k, \theta_k, u_k), \quad y \in \mathbf{R} \tag{1}$$

where x is the state, θ is the parameter, u is the input, k is the time step, y is the output, and f and h are the nonlinear state and output equations. The model is herein considered as single input and single output, since for most battery electrical models the only input is current and the only output is voltage. The number of states and parameters could be larger than 1. It is noted here that the parameter θ include only those that remain to be determined. The known parameters are treated as implicit parts of the state and output equations.

In control practice, the unknown states and parameters are typically estimated based on output measurement. It is easy to conceive that the information contained in the output will determine the quality of estimation. The Fisher information matrix, which is based on the sensitivity (or derivative) of the output to each state/parameter, is a way to quantify this relationship.[46] Given a series of output measurements over time instants $t_1, t_2, \ldots t_N$,

$$Y = \begin{bmatrix} y_1 & y_2 & \cdots & y_N \end{bmatrix}^T, \tag{2}$$

the Fisher information matrix can be practically calculated as[47,50]

$$F_{info} = \frac{1}{\sigma_y^2} \left(\frac{\partial Y}{\partial(x, \theta)} \right)^T \left(\frac{\partial Y}{\partial(x, \theta)} \right), \tag{3}$$

where σ_y^2 is the variance of the output measurement error which is assumed to be Gaussian, and

$$\frac{\partial Y}{\partial(x, \theta)} = \begin{bmatrix} \left.\frac{\partial y}{\partial x_1}\right|_{t_1}, & \left.\frac{\partial y}{\partial x_2}\right|_{t_1}, & \cdots & \left.\frac{\partial y}{\partial x_n}\right|_{t_1}, & \left.\frac{\partial y}{\partial \theta_1}\right|_{t_1}, & \left.\frac{\partial y}{\partial \theta_2}\right|_{t_1}, & \cdots & \left.\frac{\partial y}{\partial \theta_m}\right|_{t_1} \\ \left.\frac{\partial y}{\partial x_1}\right|_{t_2}, & \left.\frac{\partial y}{\partial x_2}\right|_{t_2}, & \cdots & \left.\frac{\partial y}{\partial x_n}\right|_{t_2}, & \left.\frac{\partial y}{\partial \theta_1}\right|_{t_2}, & \left.\frac{\partial y}{\partial \theta_2}\right|_{t_2}, & & \left.\frac{\partial y}{\partial \theta_2}\right|_{t_2} \\ & & \cdots & & \cdots & & & \\ \left.\frac{\partial y}{\partial x_1}\right|_{t_N}, & \left.\frac{\partial y}{\partial x_2}\right|_{t_N}, & \cdots & \left.\frac{\partial y}{\partial x_n}\right|_{t_N}, & \left.\frac{\partial y}{\partial \theta_1}\right|_{t_N}, & \left.\frac{\partial y}{\partial \theta_2}\right|_{t_N}, & \cdots & \left.\frac{\partial y}{\partial \theta_n}\right|_{t_N} \end{bmatrix} \tag{4}$$

is the sensitivity matrix consisting of the partial derivatives of the output to each state/parameter at each time instant. The final form of F_{info} can be obtained as

$$F_{info} = \frac{1}{\sigma_y^2} \begin{bmatrix} \sum_{k=1}^{N}\left(\left.\frac{\partial y}{\partial x_1}\right|_{t_k}\right)^2 & \sum_{k=1}^{N}\left(\left.\frac{\partial y}{\partial x_1}\right|_{t_k}\left.\frac{\partial y}{\partial x_2}\right|_{t_k}\right) & \cdots & \sum_{k=1}^{N}\left(\left.\frac{\partial y}{\partial x_1}\right|_{t_k}\left.\frac{\partial y}{\partial x_n}\right|_{t_k}\right) & \sum_{k=1}^{N}\left(\left.\frac{\partial y}{\partial x_1}\right|_{t_k}\left.\frac{\partial y}{\partial \theta_1}\right|_{t_k}\right) & \sum_{k=1}^{N}\left(\left.\frac{\partial y}{\partial x_1}\right|_{t_k}\left.\frac{\partial y}{\partial \theta_2}\right|_{t_k}\right) & \cdots & \sum_{k=1}^{N}\left(\left.\frac{\partial y}{\partial x_1}\right|_{t_k}\left.\frac{\partial y}{\partial \theta_m}\right|_{t_k}\right) \\ * & \sum_{k=1}^{N}\left(\left.\frac{\partial y}{\partial x_2}\right|_{t_k}\right)^2 & \cdots & \sum_{k=1}^{N}\left(\left.\frac{\partial y}{\partial x_2}\right|_{t_k}\left.\frac{\partial y}{\partial x_n}\right|_{t_k}\right) & \sum_{k=1}^{N}\left(\left.\frac{\partial y}{\partial x_2}\right|_{t_k}\left.\frac{\partial y}{\partial \theta_1}\right|_{t_k}\right) & \sum_{k=1}^{N}\left(\left.\frac{\partial y}{\partial x_2}\right|_{t_k}\left.\frac{\partial y}{\partial \theta_2}\right|_{t_k}\right) & \cdots & \sum_{k=1}^{N}\left(\left.\frac{\partial y}{\partial x_1}\right|_{t_k}\left.\frac{\partial y}{\partial \theta_m}\right|_{t_k}\right) \\ * & * & \cdots & \cdots & \cdots & & & \cdots \\ * & * & \cdots & \sum_{k=1}^{N}\left(\left.\frac{\partial y}{\partial x_n}\right|_{t_k}\right)^2 & \sum_{k=1}^{N}\left(\left.\frac{\partial y}{\partial x_n}\right|_{t_k}\left.\frac{\partial y}{\partial \theta_1}\right|_{t_k}\right) & \sum_{k=1}^{N}\left(\left.\frac{\partial y}{\partial x_n}\right|_{t_k}\left.\frac{\partial y}{\partial \theta_2}\right|_{t_k}\right) & \cdots & \sum_{k=1}^{N}\left(\left.\frac{\partial y}{\partial x_n}\right|_{t_k}\left.\frac{\partial y}{\partial \theta_m}\right|_{t_k}\right) \\ * & * & \cdots & * & \sum_{k=1}^{N}\left(\left.\frac{\partial y}{\partial \theta_1}\right|_{t_k}\right)^2 & \sum_{k=1}^{N}\left(\left.\frac{\partial y}{\partial \theta_1}\right|_{t_k}\left.\frac{\partial y}{\partial \theta_2}\right|_{t_k}\right) & \cdots & \sum_{k=1}^{N}\left(\left.\frac{\partial y}{\partial \theta_1}\right|_{t_k}\left.\frac{\partial y}{\partial \theta_m}\right|_{t_k}\right) \\ * & * & \cdots & * & * & \sum_{k=1}^{N}\left(\left.\frac{\partial y}{\partial \theta_2}\right|_{t_k}\right)^2 & \cdots & \sum_{k=1}^{N}\left(\left.\frac{\partial y}{\partial \theta_2}\right|_{t_k}\left.\frac{\partial y}{\partial \theta_m}\right|_{t_k}\right) \\ * & * & \cdots & * & * & \cdots & \cdots & \cdots \\ * & * & \cdots & * & * & * & \cdots & \sum_{k=1}^{N}\left(\left.\frac{\partial y}{\partial \theta_m}\right|_{t_k}\right)^2 \end{bmatrix}, \tag{5}$$

where $*$ denotes the symmetric entry. It is seen that the Fisher information matrix evaluates the quality of estimation by considering the noise level of the output measurements and the information contained in the data (featured by sensitivity of the output to the state/parameter).

The Fisher information matrix can be used to evaluate the identifiability of the state/parameter from the data in various ways. For example, in Ref. 47, the minimum eigenvalue of F_{info} is compared to a threshold to determine identifiability, and in Ref. 52, the determinant of F_{info} is used as the criterion. However, it is difficult to demonstrate the identifiability intuitively by using the Fisher information matrix directly, as neither its eigenvalue nor determinant has clear physical insight. An alternative is the Cramer-Rao bound,[53] which establishes that the covariance of the estimation by an unbiased estimator is bounded from below by the inverse of F_{info} evaluated at the actual values x and θ,

$$\text{cov}_{est} \geq F_{info}^{-1}(x, \theta). \qquad [6]$$

Specifically, the diagonal element of F_{info}^{-1} prescribes the lower bound of the variance for each state/parameter estimate, $\sigma^2(\hat{x}_j)$, $j = 1, 2, \ldots n$, or $\sigma^2(\hat{\theta}_j)$, $j = 1, 2, \ldots m$. The normalized standard deviation (SD), $\bar{\sigma}(\hat{x}_j)$ or $\bar{\sigma}(\hat{\theta}_j)$, which represents the ratio of the expected error SD to the true value, can be obtained by dividing $\sigma(\hat{x}_j)$ or $\sigma(\hat{\theta}_j)$ with x_j or θ_j.

The Cramer-Rao bound is capable of predicting the best-case variance of the state/parameter estimation based on the knowledge of the variance of the output measurement σ_y^2 and the correlation between the output and the state/parameter specified by the partial derivatives. The Cramer-Rao bound was derived independent of any specific form of observers, and it specifies the minimum achievable variance by any unbiased estimator. It needs to be acknowledged that impacts of the unmodeled system dynamics, which are inevitable for most modeling approaches, have not been considered in this framework. Indeed, unmodeled system dynamics will increase the error on top of the bounds analytically derived in this paper.

Derivation of the Cramer-Rao Bound for Battery SOC, Capacity and Resistance Estimation

In this section, the analytic expression of the Cramer-Rao bound on the battery state and parameter estimation will be derived based on the equivalent circuit model,[12–15] which is the most widely used in control practice and whose structural identifiability has been established in Ref. 58. The considered state is the battery SOC, and the parameters are the capacity Q and (ohmic) resistance R. The sensitivity of the measured voltage to the state/parameter will first be derived. The Cramer-Rao bound will then be derived for three different estimation schemes, namely

1) standalone estimation, i.e. only one state/parameter is being estimated.
2) combined estimation of two state/parameters simultaneously, and
3) combined estimation of three state/parameters simultaneously.

In standalone estimation, the assumption is that all the other state/parameters are perfectly known, and the data is used to identify the one state/parameter solely. When multiple state/parameters are unknown, they all need to be identified and such case will be discussed in the combined estimation. It will also be shown how large the estimation error will be if one parameter is identified by assuming erroneous values for other state/parameters as comparison. The conclusions will demonstrate how the estimation accuracy is affected by the characteristics of the data such as the SOC variation, number of data points, slope of OCV and current magnitude among others.

Sensitivity of voltage measurement to battery state/parameters.— Typically, the equivalent circuit model uses an open circuit voltage, a series resistance, and resistance-capacitor (R-C) pair(s) to capture the voltage dynamics of a battery cell, as shown in Figure 1. The open circuit voltage represents the potential difference between the cathode and the anode of the cell, which is a function of battery SOC. The
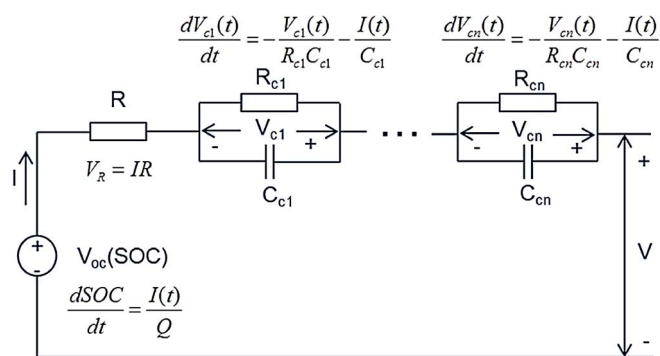

Figure 1. Schematic of the Equivalent Circuit Model.

series resistance R captures the lumped ohmic resistance of both the solid and liquid phases of the cell material. The R-C pairs are used to approximate the voltage transient behaviors such as the dynamics of the SEI film, dynamics of the charge-transfer resistance and the double layer capacitance, and lithium ion diffusion.[13] The accuracy of the approximation typically improves with the number of R-C pairs at the cost of computational complexity, and the optimal number varies among battery chemistries. To preserve generality, a general number n is considered in this paper. The governing equations of the equivalent circuit model usually take the form

$$\frac{dSOC(t)}{dt} = \frac{I(t)}{Q}$$

$$\frac{dV_{cj}(t)}{dt} = -\frac{V_{cj}(t)}{R_{cj}C_{cj}} - \frac{I(t)}{C_{cj}},$$

$$V(t) = g(SOC) + \sum_{j=1}^{n} V_{cj}(t) + I(t)R \qquad [7]$$

where I is the current, Q is the battery capacity (could be lumped with the charging/discharging efficiency), and R_{cj} and C_{cj} are the coefficients of the R-C pairs. The ohmic resistance R is assumed to be a constant for simplicity although it may change with SOC for some batteries. Parameter values are usually different for different battery chemistries, and no specific numbers are assumed throughout derivation for generality. It is noted that not all battery models have an explicit form as that in Equation 7, e.g. the electrochemical model[18,19] consisting of four partial differential equations capturing solid and liquid phase lithium concentration and potential, and an algebraic constraint (Butler-Volmer equation). Nevertheless, the conclusions obtained based on the equivalent circuit model are still enlightening for the analysis of electrochemical model since the two are closely related. On one hand, it has been shown in Refs. 21 and 22 that the electrochemical model can be reduced to a "single particle" model which is in an explicit form essentially the same as that of the equivalent circuit model. The state of charge calculated by coulomb counting in the equivalent circuit model represents the bulk/surface concentration of the lithium ion stored in the particle. The series resistance R is the sum of the resistance of the electrolyte, electrode film and current collectors. The capacity is associated with the amount of active materials that could store lithium ion. The conclusions later derived in the paper, such as the contributing factors of the data set to the estimation accuracy, can be used to guide the experiment design for estimating those parameters in the electrochemical model. On the other hand, although phenomenological as it appears, the equivalent circuit model is often derived based on electrochemical measurement directly. For example, constant phase elements have been widely used to model battery electrochemical behavior by using electrochemical impedance spectroscopy (EIS) data.[13] The final form of such model in time domain is realized as the equivalent circuit model.

The state/parameter estimation problem is defined as determining some or all of SOC, Q and R based on measurements of current $I(t)$ and voltage $V(t)$ over a period of time $[t_0, t_f]$. In practice, however, the measurements can only be obtained as sampled signals at discrete time instants. Hence it is necessary to transform the continuous differential Equation 7 to discrete time equation[57] as

$$
\begin{bmatrix} SOC_{k+1} \\ V_{c1,k+1} \\ \cdots \\ V_{cn,k+1} \end{bmatrix} = \begin{bmatrix} 1 & 0 & \cdots \\ 0 & e^{\frac{-\Delta t}{R_{c1}C_{c1}}} & \\ & \cdots & \\ 0 & \cdots & e^{\frac{-\Delta t}{R_{cn}C_{cn}}} \end{bmatrix} \begin{bmatrix} SOC_k \\ V_{c1,k} \\ \cdots \\ V_{cn,k} \end{bmatrix}
$$
$$
+ \begin{bmatrix} \frac{\Delta t}{Q} \\ -R_{c1}(1 - e^{\frac{-\Delta t}{R_{c1}C_{c1}}}) \\ \cdots \\ -R_{cn}(1 - e^{\frac{-\Delta t}{R_{cn}C_{cn}}}) \end{bmatrix} I_k,
$$
[8]
$$
V_k = g(SOC_k) + \sum_{j=1}^{n} V_{cj} + I_k R
$$

where the subscript k denotes the time step, and Δt is the sampling period. The sampling period Δt is determined by the specifications of the voltage and current sensors and the requirement on estimation accuracy, which is typically 10 ms in the battery management systems. Shorter sampling time will yield higher estimation accuracy at the cost of increased hardware and computational overhead. Number of data points collected for estimation will also affect the estimation accuracy. It will be shown later in the derivation that as the number of data points increases, the variance the estimation error will decrease, showing improved estimation accuracy.

Suppose that the initial battery SOC is SOC_0, the SOC at time instant t_k can be obtained based on Eq. 8 as,

$$
SOC_k = SOC_0 + \sum_{i=1}^{k-1} \frac{I_i \Delta t}{Q} \tag{9}
$$

and hence V_k will be

$$
V_k = g\left(SOC_0 + \sum_{i=1}^{k-1} \frac{I_i \Delta t}{Q}\right) + I_k R + \sum_{i=1}^{k-1}\sum_{j=1}^{n} R_{cj} I_i (1 - e^{\frac{-\Delta t}{R_{cj}C_{cj}}}).
$$
[10]

The sensitivity of the voltage to each state/parameter at each time instant, i.e. the partial derivatives $\frac{\partial V}{\partial SOC}|_{t_k}$, $\frac{\partial V}{\partial Q}|_{t_k}$, and $\frac{\partial V}{\partial R}|_{t_k}$ can be obtained as

$$
\left.\frac{\partial V}{\partial SOC_0}\right|_{t_k} = \alpha, \tag{11a}
$$

$$
\left.\frac{\partial V}{\partial Q}\right|_{t_k} = -\frac{\alpha}{Q^2} \sum_{i=1}^{k-1} I_i \Delta t, \tag{11b}
$$

$$
\left.\frac{\partial V}{\partial R}\right|_{t_k} = I_k, \tag{11c}
$$

where α is the slope of the function g (mainly OCV). It is noted that the slope of OCV is constant for most battery chemistries within the normal operation range and hence α is treated as a fixed value here. For example, the OCV of two lithium ion battery chemistries, LiNiMnCo (NMC) and LiFePO4 (LFP), are plotted in Figure 2. It can be seen that both OCVs can be approximated very well by piece-wise linear segments, and the slope of OCV is nearly constant in the normal operation range of 10%-90% SOC, i.e. 0.65 V/100% for NMC and 0.17 V/100% for LFP. These two battery chemistries will be used as examples to analyze the results later. The equivalent circuit model of them have been parameterized and validated in Refs. 12 and 56 respectively, and their model parameters under 25°C ambient
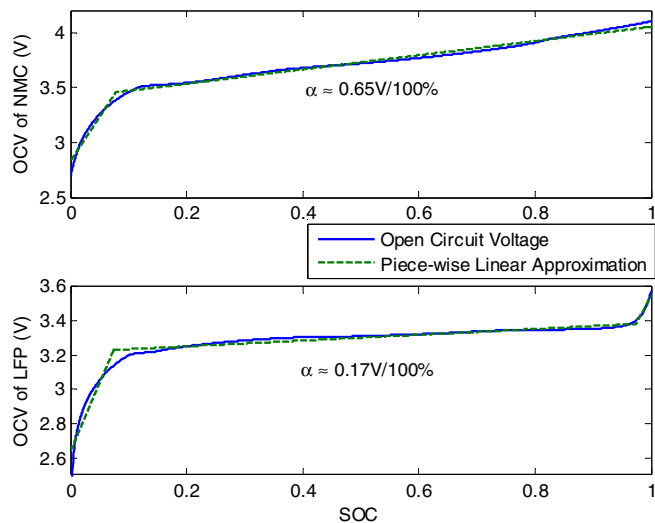

Figure 2. Open Circuit Voltage of LFP and NMC battery.

are listed in Table I. The subsequent derivation only requires slight modification even if α is considered as SOC-dependent.

Cramer-Rao bound for standalone estimation.— The state/ parameter is estimated given a series of voltage and current measurements, $\mathbf{V} = [V_1 \ V_2 \ \dots \ V_N]^T$ and $\mathbf{I} = [I_1 \ I_2 \ \dots \ I_N]^T$, collected over time instants $t_1, t_2, \dots t_N$.

When only SOC is being estimated, the Fisher information matrix can be derived based on Eq. 5 and Eq. 11a as

$$
F_{\text{info}} = \frac{1}{\sigma_V^2} \sum_{i=1}^{N} \left(\left.\frac{\partial V}{\partial SOC_0}\right|_{t_k}\right)^2 = \frac{N\alpha^2}{\sigma_V^2}, \tag{12}
$$

where σ_V^2 is the variance of the voltage measurement noises. The Cramer-Rao bound for SOC estimation is then

$$
\sigma(\hat{SOC_0}) \geq F_{\text{info}}^{-\frac{1}{2}} = \frac{\sigma_V}{\alpha\sqrt{N}}. \tag{13}
$$

Note 1: As expected, the SD of estimation error is proportional to that of the measurement noise.

Note 2: The accuracy will improve under larger slope of the OCV and more data points used for estimation. For SOC estimation, most online recursive algorithms use one voltage measurement each time for SOC estimation ($N = 1$), and $\bar{\sigma}(\hat{SOC_0})$ will hence be 1.54% for NMC battery (using $\alpha = 0.65V/100\%$ in the middle SOC range as listed in Table I) and 5.88% for LFP battery (using $\alpha = 0.17V/100\%$ in the middle SOC range in Table I) assuming $\sigma_V = 10mV$. This agrees with the intuition that steeper OCV is conducive to high SOC estimation accuracy.

Table I. Model Parameters of LiFePO4 (LFP) and LiNiMnCo Batteries (25°C ambient).

OCV	LiFePO4 Figure 2a	LiNiMnCo Figure 2b
α (OCV slope, middle SOC range)	1.7 mV/1% SOC	6.5 mV/1% SOC
Q	2.3 Ah	5 Ah
R	10 mΩ	2 mΩ
R_{c1}	15 mΩ	0.8 mΩ
C_{c1}	2.4 kF	6 kF
R_{c2}	20 mΩ	1 mΩ
C_{c2}	70 kF	4 kF

When only the capacity Q is being estimated, the Fisher information matrix can be derived based on Eq. 5 and Eq. 11b as

$$F_{info} = \frac{1}{\sigma_V^2} \sum_{k=1}^{N} \left(\frac{\partial V}{\partial Q} \Big|_{t_k} \right)^2 = \frac{1}{\sigma_V^2} \frac{\alpha^2}{Q^4} \sum_{k=1}^{N} \left(\sum_{i=1}^{k-1} (I_i \Delta t) \right)^2$$

$$= \frac{\alpha^2}{\sigma_V^2 Q^2} \sum_{k=1}^{N} (\Delta SOC_k)^2, \qquad [14]$$

where $\Delta SOC_k = \frac{\sum_i^{k-1} I_i \Delta t}{Q} = SOC_k - SOC_0$ denotes the variation of SOC_k from the initial value. The normalized Cramer-Rao bound for Q estimation is then

$$\bar{\sigma} \left(\hat{Q} \right) \geq F_{info}^{-\frac{1}{2}} / Q = \frac{\sigma_V}{\alpha \sqrt{\sum_{k=1}^{N} (\Delta SOC_k)^2}}. \qquad [15]$$

Note 1: The noise level in voltage measurement has a proportional effect on the estimation accuracy.

Note 2: The accuracy of capacity estimation will improve under higher OCV slope α and larger SOC variation in the data set $\sqrt{\sum_{k=1}^{N} (\Delta SOC_k)^2}$. Assume two voltage measurements are used for capacity estimation, one at 10% SOC and the other at 90% SOC (amount to SOC variation of 80%), $\bar{\sigma}(\hat{Q})$ will be 1.92% for NMC battery and 7.35% for LFP battery when $\sigma_V = 10\,mV$. If the SOC variation is down to 40%, $\bar{\sigma}(\hat{Q})$ will increase to 3.85% and 14.71% for NMC and LFP respectively.

When only the resistance R is being estimated, the Fisher information matrix can be derived based on Eq. 5 and Eq. 11c as

$$F_{info} = \frac{1}{\sigma_V^2} \sum_{k=1}^{N} \left(\frac{\partial V}{\partial R} \Big|_{t_k} \right)^2 = \frac{1}{\sigma_V^2} \sum_{k=1}^{N} (I_k)^2. \qquad [16]$$

The normalized Cramer-Rao bound for R estimation is then

$$\bar{\sigma} \left(\hat{R} \right) \geq F_{info}^{-\frac{1}{2}} / R = \frac{\sigma_V}{R \sqrt{\sum_{k=1}^{N} (I_k)^2}}. \qquad [17]$$

Note 1: Similar to the previous cases, SD of the estimation error is proportional to the noise level in voltage measurement.

Note 2: The accuracy of resistance estimation will improve under high current $\sqrt{\sum_{k=1}^{N} (I_k)^2}$, which is easy to understand as higher current will result in larger voltage change from OCV. The normalized error SD will also be smaller for battery with larger nominal resistance. Take the NMC and LFP batteries as examples, whose nominal resistances are $2\,m\Omega$ and $10\,m\Omega$ respectively, when a single measurement is used for estimation under $I = 20A$, $\bar{\sigma}(\hat{R})$ will be 25% for NMC battery and 5% for LFP battery assuming $\sigma_V = 10\,mV$.

In summary, for all three state/parameters, the SD of the estimation will improve under smaller measurement noise σ_V. Other contributing factors to estimation accuracy includes the slope of OCV curve α, number of data points N, current variation $\sum_{k=1}^{N} (I_k)^2$, and SOC variation $\sum_{k=1}^{N} (\Delta SOC_k)^2$. Specifically, SOC estimation improves under larger α and N, capacity estimation favors larger α and $\sum_{k=1}^{N} (\Delta SOC_k)^2$, and resistance estimation prefers larger $\sum_{k=1}^{N} (I_k)^2$. Large N will also improve the estimation accuracy of Q and R as $\sum_{k=1}^{N} (\Delta SOC_k)^2$ and $\sum_{k=1}^{N} (I_k)^2$ will

increase accordingly. Ideally, the SD of the estimation error could be arbitrarily small if N is large sufficiently. However, the computational load to process the data will also increase drastically and hence impose a practical limit. These conclusions confirm the long existing intuition on the factors affecting estimation accuracy, and more importantly, also provide theoretical and quantifiable correlations between the variance of the estimate and these factors.

Cramer-Rao bound for combined estimation of two state/parameters.— In this subsection, three cases of combined estimation will be discussed, including combined SOC/Q estimation, combined SOC/R estimation, and combined Q/R estimation. The significance of exploring the accuracy of combined estimation is explained as follows. When one state/parameter, e.g. SOC, needs to be estimated with some others also unknown, e.g. capacity, there are typically two ways of conducting the estimation. The first one is to estimate all the unknown state/parameters with the data obtained (combined estimation), and the other one is to only estimate the interested one while assuming nominal values for the other unknown ones (standalone estimation with imperfect parameters). The second way will usually lead to large estimation error as to be shown, which inspires the extensive research on combined estimation documented in literature. For combined estimation, it will be shown that under common current inputs, the accuracy of combined estimation usually degrades as compared to that of standalone estimation. However, when the current input is designed to satisfy certain patterns, such loss of accuracy can be avoided.

When both SOC and capacity Q need to be estimated, the Fisher information matrix can be derived based on Eq. 5, Eq. 11a and Eq. 11b as

$$F_{info} = \frac{1}{\sigma_V^2} \begin{bmatrix} \sum_{k=1}^{N} \left(\frac{\partial V}{\partial SOC_0} \Big|_{t_k} \right)^2 & \sum_{k=1}^{N} \left(\frac{\partial V}{\partial SOC_0} \Big|_{t_k} \frac{\partial V}{\partial Q} \Big|_{t_k} \right) \\ \sum_{k=1}^{N} \left(\frac{\partial V}{\partial SOC_0} \Big|_{t_k} \frac{\partial V}{\partial Q} \Big|_{t_k} \right) & \sum_{k=1}^{N} \left(\frac{\partial V}{\partial Q} \Big|_{t_k} \right)^2 \end{bmatrix}$$

$$= \frac{1}{\sigma_V^2} \begin{bmatrix} N\alpha^2 & -\frac{\alpha^2}{Q} \sum_{k=1}^{N} (\Delta SOC_k) \\ -\frac{\alpha^2}{Q} \sum_{k=1}^{N} (\Delta SOC_k) & \frac{\alpha^2}{Q^2} \sum_{k=1}^{N} (\Delta SOC_k)^2 \end{bmatrix}. \qquad [18]$$

The normalized Cramer-Rao bounds for combined SOC and capacity estimation are then

$$\bar{\sigma}_{SOC,Q} \left(S\hat{O}C_0 \right) \geq \frac{\sigma_V}{\alpha \sqrt{N}} \frac{1}{\sqrt{1 - \frac{\left(\sum_{k=1}^{N} \Delta SOC_k \right)^2}{N \sum_{k=1}^{N} (\Delta SOC_k)^2}}}$$

$$\bar{\sigma}_{SOC,Q} \left(\hat{Q} \right) \geq \frac{\sigma_V}{\alpha \sqrt{\sum_{k=1}^{N} (\Delta SOC_k)^2}} \frac{1}{\sqrt{1 - \frac{\left(\sum_{k=1}^{N} \Delta SOC_k \right)^2}{N \sum_{k=1}^{N} (\Delta SOC_k)^2}}}. \qquad [19]$$

where the subscript SOC, Q denotes the combined SOC and Q estimation.

Interestingly, it is noticed that the SDs of the estimates are amplified by a factor of $\frac{1}{\sqrt{1 - \frac{\left(\sum \Delta SOC_k \right)^2}{N \sum (\Delta SOC_k)^2}}}$ as compared to those in standalone
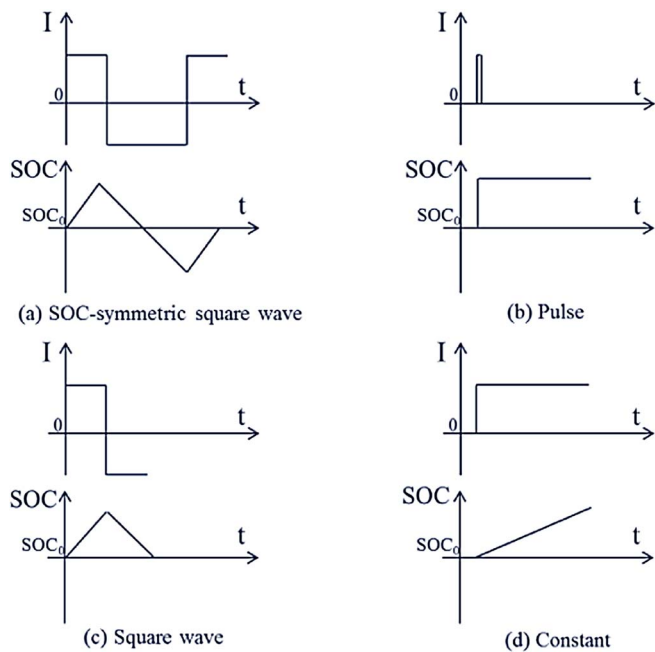
Figure 3. Examples of Current Input Profile.

estimation shown in Eq. 13 and Eq. 15, which is in the range of

$$1 \le \frac{1}{\sqrt{1 - \dfrac{\left(\sum\limits_{k=1}^{N} \Delta SOC_k\right)^2}{N \sum\limits_{k=1}^{N} (\Delta SOC_k)^2}}} \le \infty. \qquad [20]$$

The amplification factor will be equal to 1, meaning no loss of accuracy, when the SOC variation ΔSOC_k is a zero-sum sequence, for example, under the SOC-symmetric square-wave current shown in

Figure 3a. The amplification factor will be infinite, indicating no identifiability, when ΔSOC_k is constant, e.g. under a single pulse shown in Figure 3b. It can be concluded that

* the accuracy of the combined SOC/Q estimation will never exceed that of the standalone estimation;
* SOC variation is required for combined SOC/Q estimation as the variance of the estimate will be infinite under zero SOC variation, and larger SOC variation will reduce the loss of accuracy;
* it is possible to avoid loss of accuracy under combined SOC/Q estimation if the current profile is designed such that the SOC variation is zero-sum over time.

In order to illustrate the derived results numerically, the SOC estimation errors of different estimation schemes for NMC and LFP batteries under square-wave current (plotted in Figure 3c) are calculated and shown in Figure 4. The example data sets contain 8 measurement points (N = 8); current $I = \pm 1C$, which is 5 A for NMC whose capacity is 5 Ah, and 2.3 A for LFP whose capacity is 2.3 Ah; SOC varies from 10% to around 90%; and the OCV slope in the middle SOC range ($\alpha = 6.5\,mV/1\%$ for NMC and $\alpha = 1.7\,mV/1\%$ for LFP) are used. It is seen that under combined SOC and Q estimation, the error SD $\bar{\sigma}_{soc}$ is 0.94% for NMC and 3.56% for LFP (second group in Figure 4), increasing from 0.59% for NMC and 2.22% for LFP under standalone estimation with perfect knowledge of capacity Q (first group in Figure 4). The estimation errors of standalone SOC estimation with erroneous Q (biased by 10%) is also calculated based on Monte Carlos simulation and shown in Figure 4 (the fifth group). It is seen that imperfect knowledge of capacity will lead to larger errors in SOC estimation, i.e. 3.37% mean (bias) error and 0.58% error SD (random) for NMC and 3.37% mean error and 2.23% error SD for LFP. The overall estimation error is larger than the combined SOC and Q estimation, which does not suffer from mean error (bias). The capacity estimation errors for different estimation schemes are shown in Figure 5. Similar to SOC estimation, it can be seen that under square-wave current, the capacity estimation accuracy of the combined SOC and Q estimation (the second group) will deteriorate compared to that of standalone estimation with perfect knowledge of SOC (the first group), but still better than that of standalone estimation when SOC is not accurately known (the fifth group).
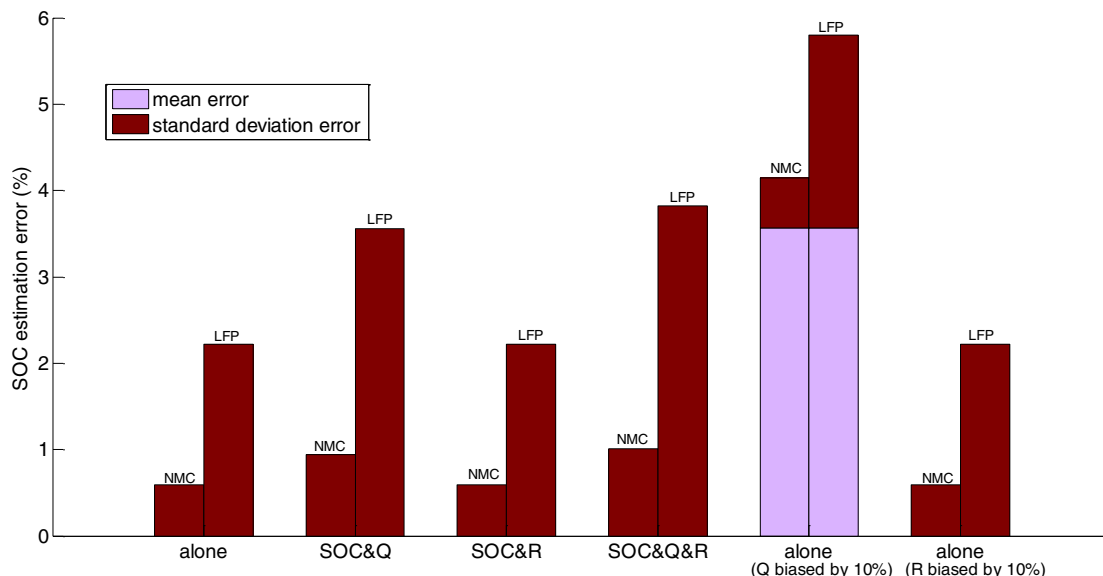

Figure 4. SOC estimation errors of different estimation schemes under square-wave current.
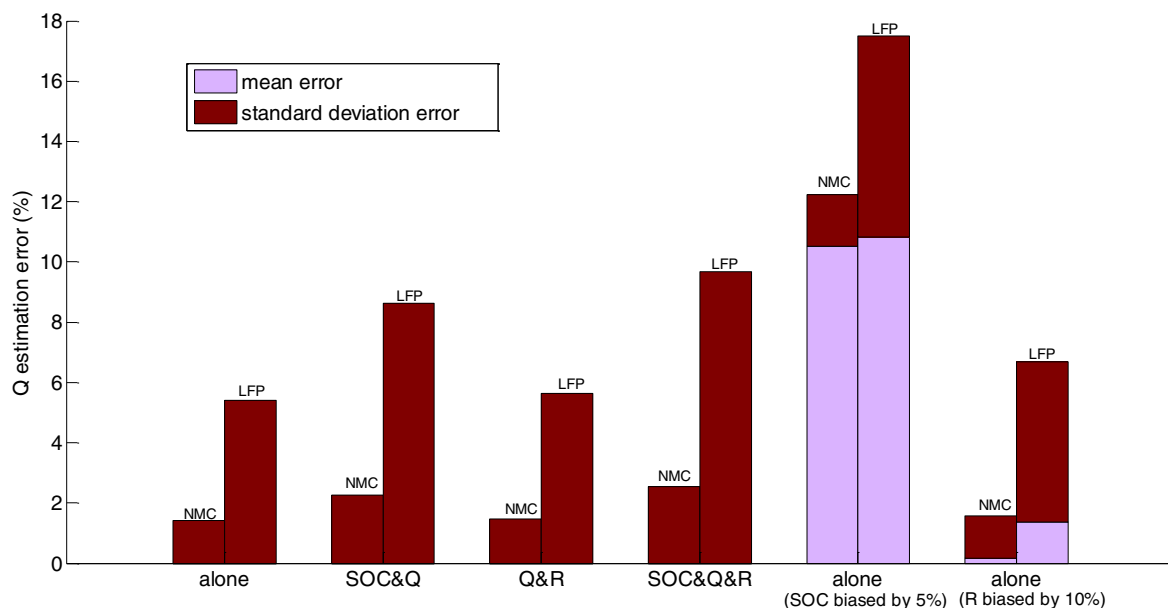
Figure 5. Capacity estimation errors of different estimation schemes under square-wave current.

When both SOC and resistance R need to be estimated, the Fisher information matrix can be derived based on Eq. 5, Eq. 11a and Eq. 11c as

$$F_{\text{info}} = \frac{1}{\sigma_V^2} \begin{bmatrix} \sum_{k=1}^{N} \left(\left. \frac{\partial V}{\partial SOC_0} \right|_{t_k} \right)^2 & \sum_{k=1}^{N} \left(\left. \frac{\partial V}{\partial SOC_0} \right|_{t_k} \left. \frac{\partial V}{\partial R} \right|_{t_k} \right) \\ \sum_{k=1}^{N} \left(\left. \frac{\partial V}{\partial SOC_0} \right|_{t_k} \left. \frac{\partial V}{\partial R} \right|_{t_k} \right) & \sum_{k=1}^{N} \left(\left. \frac{\partial V}{\partial R} \right|_{t_k} \right)^2 \end{bmatrix}$$

$$= \frac{1}{\sigma_V^2} \begin{bmatrix} N\alpha^2 & \alpha \sum_{k=1}^{N} (I_k) \\ \alpha \sum_{k=1}^{N} (I_k) & \sum_{k=1}^{N} (I_k)^2 \end{bmatrix}. \qquad [21]$$

The normalized Cramer-Rao bounds for combined SOC and resistance estimation are then

$$\bar{\sigma}_{SOC,R} \left(S\hat{O}C_0 \right) \geq \frac{\sigma_V}{\alpha \sqrt{N}} \frac{1}{\sqrt{1 - \frac{\left(\sum_{k=1}^{N} I_k \right)^2}{N \sum_{k=1}^{N} (I_k)^2}}}$$

$$\qquad [22]$$

$$\bar{\sigma}_{SOC,R} \left(\hat{R} \right) \geq \frac{\sigma_V}{R \sqrt{\sum_{k=1}^{N} (I_k)^2}} \frac{1}{\sqrt{1 - \frac{\left(\sum_{k=1}^{N} I_k \right)^2}{N \sum_{k=1}^{N} (I_k)^2}}},$$

the subscript SOC, R denotes the combined SOC and R estimation.

It is noticed that the standard deviations of the estimates are amplified by a factor of $\dfrac{1}{\sqrt{1 - \frac{\left(\sum_{k=1}^{N} I_k \right)^2}{N \sum_{k=1}^{N} (I_k)^2}}}$ as compared to those in standalone estimation shown in Eq. 13 and Eq. 17. It can be easily shown that the amplification factor is bounded by

$$1 \leq \frac{1}{\sqrt{1 - \frac{\left(\sum_{k=1}^{N} I_k \right)^2}{N \sum_{k=1}^{N} (I_k)^2}}} \leq \infty. \qquad [23]$$

The amplification factor will be equal to 1, meaning no loss of accuracy, when the current sequence I_k is zero-sum, for example, the square-wave shown in Figure 3c. The amplification factor will be infinite, indicating no identifiability, when I_k is constant, shown in Figure 3d. It can be concluded that

• the accuracy of combined SOC and R estimation will never exceed that of the standalone estimation;
• current variation is required for combined SOC and R estimation as the variance of the estimate will be infinite under constant current, and larger current variation will reduce the loss of accuracy;
• it is possible to avoid loss of accuracy under combined SOC and R estimation if the current profile is designed to be zero-sum over time.

For numerical illustration, the SOC estimation errors of the combined SOC and R estimation using the previous data set are calculated and shown in Figure 4 (the third group). It is seen that under the square-wave current, the SOC error standard deviation is the same as that of standalone SOC estimation (for both NMC and LFP), which agrees with the above conclusion that loss of accuracy can be avoided with square-wave current. The same observation can be made for resistance estimation shown in Figure 6 (comparing first group with the second group).

When both capacity Q and resistance R need to be estimated, the Fisher information matrix can be derived based on Eq. 5, Eq. 11b and
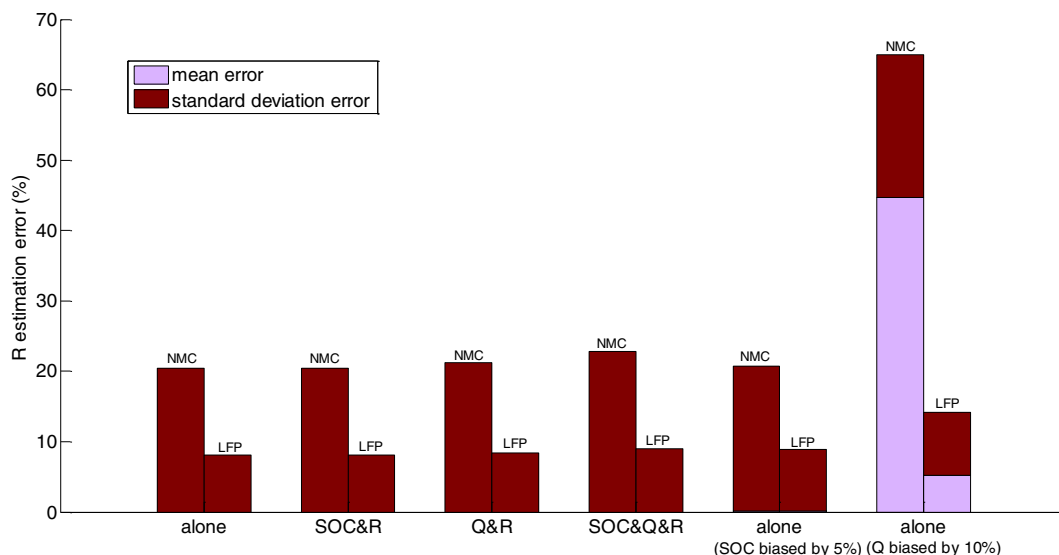
Figure 6. Resistance estimation errors of different estimation schemes under square-wave current.

Eq. 11c as

$$
F_{\text{info}} = \frac{1}{\sigma_V^2} \begin{bmatrix} \sum\limits_{k=1}^{N} \left(\left. \frac{\partial V}{\partial Q} \right|_{t_k} \right)^2 & \sum\limits_{k=1}^{N} \left(\left. \frac{\partial V}{\partial Q} \right|_{t_k} \left. \frac{\partial V}{\partial R} \right|_{t_k} \right) \\ \sum\limits_{k=1}^{N} \left(\left. \frac{\partial V}{\partial Q} \right|_{t_k} \left. \frac{\partial V}{\partial R} \right|_{t_k} \right) & \sum\limits_{k=1}^{N} \left(\left. \frac{\partial V}{\partial R} \right|_{t_k} \right)^2 \end{bmatrix}
$$

$$
= \frac{1}{\sigma_V^2} \begin{bmatrix} \dfrac{\alpha^2}{Q^2} \sum\limits_{k=1}^{N} (\Delta SOC_k)^2 & -\dfrac{\alpha}{Q} \sum\limits_{k=1}^{N} (I_k \Delta SOC_k) \\ -\dfrac{\alpha}{Q} \sum\limits_{k=1}^{N} (I_k \Delta SOC_k) & \sum\limits_{k=1}^{N} (I_k)^2 \end{bmatrix}. \quad [24]
$$

The normalized Cramer-Rao bounds for combined SOC and capacity estimation are then

$$
\bar{\sigma}_{Q,R} \left(\hat{Q} \right) \geq \frac{\sigma_V}{\alpha \sqrt{\sum\limits_{k=1}^{N} (\Delta SOC_k)^2}} \frac{1}{\sqrt{1 - \dfrac{\left(\sum\limits_{k=1}^{N} I_k \Delta SOC_k \right)^2}{\sum\limits_{k=1}^{N} (I_k)^2 \sum\limits_{k=1}^{N} (\Delta SOC_k)^2}}}
$$

$$
\bar{\sigma}_{Q,R} \left(\hat{R} \right) \geq \frac{\sigma_V}{R \sqrt{\sum\limits_{k=1}^{N} (I_k)^2}} \frac{1}{\sqrt{1 - \dfrac{\left(\sum\limits_{k=1}^{N} I_k \Delta SOC_k \right)^2}{\sum\limits_{k=1}^{N} (I_k)^2 \sum\limits_{k=1}^{N} (\Delta SOC_k)^2}}},
$$

[25]

where the subscript Q, R denotes the combined Q and R estimation.

It is noticed that the standard deviations of the estimates are amplified by a factor of $\dfrac{1}{\sqrt{1 - \dfrac{\left(\sum\limits_{k=1}^{N} I_k \Delta SOC_k \right)^2}{\sum\limits_{k=1}^{N} (I_k)^2 \sum\limits_{k=1}^{N} (\Delta SOC_k)^2}}}$ as compared to those in

standalone estimation shown in Eq. 15 and Eq. 17. It can be shown

that the amplification factor is bounded by

$$
1 \leq \frac{1}{\sqrt{1 - \dfrac{\left(\sum\limits_{k=1}^{N} I_k \Delta SOC_k \right)^2}{\sum\limits_{k=1}^{N} (I_k)^2 \sum\limits_{k=1}^{N} (\Delta SOC_k)^2}}} < \infty. \quad [26]
$$

The amplification factor will be equal to 1, meaning no loss of accuracy, when the product of I_k and ΔSOC_k adds up to zero over time, for example, under the square-wave current shown in Figure 3a or Figure 3c. The amplification factor will never be infinite, since it requires the sequence I_k and sequence ΔSOC_k to be linearly dependent according to the Cauchy-Schwarz Inequality. It can be concluded that

- the accuracy of combined Q/R estimation will never exceed that of the standalone estimation;
- larger variation of the product of I_k and ΔSOC_k will reduce the loss of accuracy;
- it is possible to avoid loss of accuracy under combined Q/R estimation if the current profile is designed such that the product of I_k and ΔSOC_k is zero-sum over time.

For numerical illustration, the capacity estimation errors of the combined Q and R estimation using the previous data set are calculated and shown in Figure 5 (the third group). It is seen that under the square-wave current, the SOC error standard deviation is the same as that of standalone SOC estimation (for both NMC and LFP), which agrees with the above conclusion that loss of accuracy can be avoided with square-wave current. The same observation can be made for resistance estimation shown in Figure 6 (comparing first group with the third group).

Cramer-rao bound for combined estimation of three state/parameters.— When all three state/parameters, SOC_0, capacity Q, and resistance R, need to be estimated, the Fisher information matrix can be derived based on Eq. 5, Eq. 11a, Eq. 11b and Eq. 11c as

$$
F_{\text{info}} = \frac{1}{\sigma_V^2}
\begin{bmatrix}
\sum_{k=1}^{N}\left(\left.\frac{\partial V}{\partial SOC_0}\right|_{t_k}\right)^2 & \sum_{k=1}^{N}\left(\left.\frac{\partial V}{\partial SOC_0}\right|_{t_k}\left.\frac{\partial V}{\partial Q}\right|_{t_k}\right) & \sum_{k=1}^{N}\left(\left.\frac{\partial V}{\partial SOC_0}\right|_{t_k}\left.\frac{\partial V}{\partial R}\right|_{t_k}\right) \\[3mm]
\sum_{k=1}^{N}\left(\left.\frac{\partial V}{\partial SOC_0}\right|_{t_k}\left.\frac{\partial V}{\partial Q}\right|_{t_k}\right) & \sum_{k=1}^{N}\left(\left.\frac{\partial V}{\partial Q}\right|_{t_k}\right)^2 & \sum_{k=1}^{N}\left(\left.\frac{\partial V}{\partial Q}\right|_{t_k}\left.\frac{\partial V}{\partial R}\right|_{t_k}\right) \\[3mm]
\sum_{k=1}^{N}\left(\left.\frac{\partial V}{\partial SOC_0}\right|_{t_k}\left.\frac{\partial V}{\partial R}\right|_{t_k}\right) & \sum_{k=1}^{N}\left(\left.\frac{\partial V}{\partial Q}\right|_{t_k}\left.\frac{\partial V}{\partial R}\right|_{t_k}\right) & \sum_{k=1}^{N}\left(\left.\frac{\partial V}{\partial R}\right|_{t_k}\right)^2
\end{bmatrix}
$$

$$
= \frac{1}{\sigma_V^2}
\begin{bmatrix}
N\alpha^2 & -\dfrac{\alpha^2}{Q}\sum_{k=1}^{N}(\Delta SOC_k) & \alpha\sum_{k=1}^{N}(I_k) \\[3mm]
-\dfrac{\alpha^2}{Q}\sum_{k=1}^{N}(\Delta SOC_k) & \dfrac{\alpha^2}{Q^2}\sum_{k=1}^{N}(\Delta SOC_k)^2 & -\dfrac{\alpha}{Q}\sum_{k=1}^{N}(I_k\Delta SOC_k) \\[3mm]
\alpha\sum_{k=1}^{N}(I_k) & -\dfrac{\alpha}{Q}\sum_{k=1}^{N}(I_k\Delta SOC_k) & \sum_{k=1}^{N}(I_k)^2
\end{bmatrix}. \tag{27}
$$

The normalized Cramer-Rao bounds for combined estimation are then

$$
\bar{\sigma}_{SOC,Q,R}\left(S\hat{O}C_0\right) \geq \frac{\sigma_V}{\alpha\sqrt{N}}\frac{1}{\sqrt{1-\dfrac{\left(\sum_{k=1}^{N}I_k\right)^2\sum_{k=1}^{N}(\Delta SOC_k)^2 + \left(\sum_{k=1}^{N}\Delta SOC_k\right)^2\sum_{k=1}^{N}(I_k)^2 - 2\left(\sum_{k=1}^{N}I_k\right)\left(\sum_{k=1}^{N}\Delta SOC_k\right)\left(\sum_{k=1}^{N}I_k\Delta SOC_k\right)}{N\sum_{k=1}^{N}(I_k)^2\sum_{k=1}^{N}(\Delta SOC_k)^2 - N\sum_{k=1}^{N}(I_k\Delta SOC_k)^2}}} \tag{28a}
$$

$$
\bar{\sigma}_{SOC,Q,R}\left(\hat{Q}\right) \geq \frac{\sigma_V}{\alpha\sqrt{\sum_{k=1}^{N}(\Delta SOC_k)^2}}\frac{1}{\sqrt{1-\dfrac{\left(\sum_{k=1}^{N}\Delta SOC_k\right)^2\sum_{k=1}^{N}(I_k)^2 + N\left(\sum_{k=1}^{N}I_k\Delta SOC_k\right)^2 - 2\left(\sum_{k=1}^{N}I_k\right)\left(\sum_{k=1}^{N}\Delta SOC_k\right)\left(\sum_{k=1}^{N}I_k\Delta SOC_k\right)}{N\sum_{k=1}^{N}(I_k)^2\sum_{k=1}^{N}(\Delta SOC_k)^2 - \left(\sum_{k=1}^{N}I_k\right)^2\sum_{k=1}^{N}(\Delta SOC_k)^2}}} \tag{28b}
$$

$$
\bar{\sigma}_{SOC,Q,R}\left(\hat{R}\right) \geq \frac{\sigma_V}{R\sqrt{\sum_{k=1}^{N}(I_k)^2}}\frac{1}{\sqrt{1-\dfrac{\left(\sum_{k=1}^{N}I_k\right)^2\sum_{k=1}^{N}(\Delta SOC_k)^2 + N\left(\sum_{k=1}^{N}I_k\Delta SOC_k\right)^2 - 2\left(\sum_{k=1}^{N}I_k\right)\left(\sum_{k=1}^{N}\Delta SOC_k\right)\left(\sum_{k=1}^{N}I_k\Delta SOC_k\right)}{N\sum_{k=1}^{N}(I_k)^2\sum_{k=1}^{N}(\Delta SOC_k)^2 - \left(\sum_{k=1}^{N}\Delta SOC_k\right)^2\sum_{k=1}^{N}(I_k)^2}}} \tag{28c}
$$

where the subscript SOC, Q, R denotes the combined SOC, Q and R estimation.

Similar to the combined estimation of two state/parameters, the standard deviation of each estimate can be expressed as the baseline standard deviation under standalone estimation derived in Eq. 13, Eq. 15 or Eq. 17 multiplied by an amplification factor. It can be easily shown that all three amplification factors are bounded between 1 and infinity. The amplification factor will be equal to 1, meaning no loss of accuracy, when $\sum_{k=1}^{N} I_k = 0$, $\sum_{k=1}^{N} SOC_k = 0$, and $\sum_{k=1}^{N} I_k\Delta SOC_k = 0$, for example, under the SOC-symmetric square-wave current shown in Figure 3a. The amplification factor will be infinity, indicating no identifiability, under the same conditions as those in two-state/parameters combined estimation shown in the previous section. It is concluded that

- the accuracy of combined SOC/Q/R estimation will never exceed that of the standalone estimation;

- current variation and SOC variation are both required for combined SOC/Q/R estimation as the variance of the estimate will be infinite otherwise, e.g. under single pulse or constant current, and larger variation will reduce the loss of accuracy.

- it is possible to avoid loss of accuracy under combined SOC/Q/R estimation if the current input is designed such that the current sequence I_k, SOC variation sequence ΔSOC_k, and $I_k\Delta SOC_k$ are all zero-sum over time.

It is likely to hold but remains to be proven that the accuracy of combined SOC/Q/R estimation will never exceed that of any combined two-state/parameter estimation (need to show that the amplification factors in Eq. 28a–28c are larger than those in Eq. 19, Eq. 22 and Eq. 25).

The estimation errors of the combined SOC, Q and R estimation are shown in Figure 4, Figure 5 and Figure 6 respectively (all in the fourth group). It can be seen that the estimation accuracy deteriorates as compared to that of standalone and combined estimation. The resistance estimation does not suffer from obvious degradation though.

Table II. Cramer-Rao Bounds for Battery SOC/capacity/resistance Estimation under Generic Current Input.

		$\bar\sigma(S\hat{O}C)$	$\bar\sigma(\hat{Q})$	$\bar\sigma(\hat{R})$
Standalone Estimation		$\dfrac{\sigma_V}{\alpha\sqrt{N}}$	$\dfrac{\sigma_V}{\alpha\sqrt{\sum_{k=1}^N (\Delta SOC_k)^2}}$	$\dfrac{\sigma_V}{R\sqrt{\sum_{k=1}^N (I_k)^2}}$
Combined 2-state/ parameter Estimation	SOC/Q	$\dfrac{\sigma_V}{\alpha\sqrt{N}}\sqrt{\dfrac{1}{1-\dfrac{(\sum_{k=1}^N \Delta soc_k)^2}{N\sum_{k=1}^N (\Delta soc_k)^2}}}$	$\dfrac{\sigma_V}{\alpha\sqrt{\sum_{k=1}^N (\Delta SOC_k)^2}}\sqrt{\dfrac{1}{1-\dfrac{(\sum_{k=1}^N \Delta soc_k)^2}{N\sum_{k=1}^N (\Delta soc_k)^2}}}$	\\
	SOC/R	$\dfrac{\sigma_V}{\alpha\sqrt{N}}\sqrt{\dfrac{1}{1-\dfrac{(\sum_{k=1}^N I_k)^2}{N\sum_{k=1}^N (I_k)^2}}}$	\\	$\dfrac{\sigma_V}{R\sqrt{\sum_{k=1}^N (I_k)^2}}\sqrt{\dfrac{1}{1-\dfrac{(\sum_{k=1}^N I_k)^2}{N\sum_{k=1}^N (I_k)^2}}}$
	Q/R	\\	$\dfrac{\sigma_V}{\alpha\sqrt{\sum_{k=1}^N (\Delta SOC_k)^2}}\sqrt{\dfrac{1}{1-\dfrac{(\sum_{k=1}^N I_k\Delta SOC_k)^2}{\sum_{k=1}^N (I_k)^2 \sum_{k=1}^N (\Delta SOC_k)^2}}}$	$\dfrac{\sigma_V}{R\sqrt{\sum_{k=1}^N (I_k)^2}}\sqrt{\dfrac{1}{1-\dfrac{(\sum_{k=1}^N I_k\Delta SOC_k)^2}{\sum_{k=1}^N (I_k)^2 \sum_{k=1}^N (\Delta SOC_k)^2}}}$
Combined 3-state/parameter Estimation		Eq. 28a	Eq. 28b	Eq. 28c

All the previously derived Cramer-Rao bounds have been summarized in Table II.

Cramer-Rao Bounds for Battery SOC, Capacity and Resistance Estimation under Featured Current Inputs

In this section, the derived Cramer-Rao bounds will be evaluated under different featured current inputs, namely the constant current and square-wave current. It will be shown what the bounds are under these commonly seen currents, and how they degrade under combined estimation as compared to standalone estimation. The bounds will also be compared between different inputs.

The three considered inputs will take the form,

$$\text{constant current: } I(k) = I_0, \quad k = 1, 2, \ldots N \tag{29a}$$

$$\text{square-wave: } I(k) = \begin{cases} I_0, & k = 1, 2, \ldots \dfrac{N}{2} \\ -I_0, & k = \dfrac{N}{2} + 1, \ldots N \end{cases} \tag{29b}$$

SOC-symmetric square-wave:

$$I(k) = \begin{cases} I_0, & k = 1, 2, \ldots \dfrac{N}{4} \\ -I_0, & k = \dfrac{N}{4} + 1, \ldots \dfrac{3N}{4} \\ I_0, & k = \dfrac{3N}{4} + 1, \ldots \dfrac{N}{2} \end{cases} \tag{29c}$$

as shown in Figure 7. The Cramer-Rao bounds have been calculated and summarized in Table III for all three inputs (when the data points N are large), where the SOC swing under the constant current is
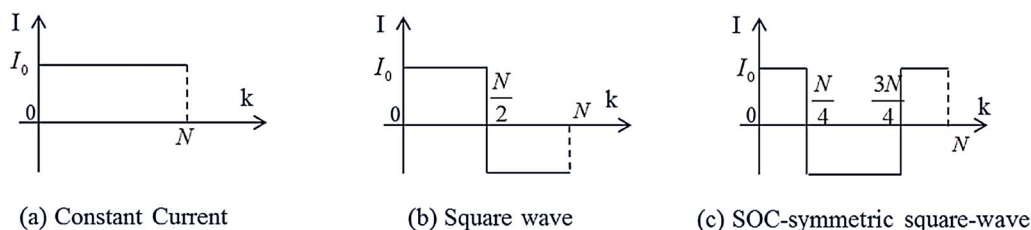
denoted as

$$\nabla SOC \triangleq \frac{N I_0 \Delta t}{Q}. \tag{30}$$

It is noted that the SOC swings under square-wave and SOC-symmetric square-wave are $\frac{\nabla SOC}{2}$ and $\frac{\nabla SOC}{4}$ respectively.

It can be concluded from Table III that

1) under constant current

- SOC cannot be estimated together with resistance, but can be estimated along with capacity at the cost of doubling the estimation error;
- capacity can be estimated together with either SOC or resistance, both at the cost of doubling the error;
- resistance cannot be estimated together with SOC, but can be estimated along with capacity with doubled estimation error;
- the three cannot be estimated altogether;
- it is noted that the above conclusions are based on the assumption of constant OCV slope α. Varying α could improve the identifiability and reduce the errors. Indeed, it has been considered in Ref. 54 to improve the accuracy of SOC estimation by introducing an abrupt change of slope on the OCV curve.

2) under square-wave current

- SOC can be estimated together with either capacity at the cost of doubling the error, or resistance without loss of accuracy;
- capacity can be estimated together with either SOC at the cost of doubling the error, or resistance without loss of accuracy;
- resistance can be estimated together with either SOC or capacity, both without loss of accuracy;
- the three can be estimated altogether, and the estimation errors for SOC and capacity will be doubled while that for resistance remains unchanged;

(a) Constant Current   (b) Square wave   (c) SOC-symmetric square-wave

Figure 7. Featured Current Inputs.

Table III. Cramer-Rao Bounds for Battery SOC/capacity/resistance Estimation under Featured Currents (under sufficiently large N).

	$\bar{\sigma}(S\hat{O}C)$			$\bar{\sigma}(\hat{Q})$			$\bar{\sigma}(\hat{R})$		
	Constant Current	Square Wave	SOC symmetric Square-Wave	Constant Current	Square Wave	SOC symmetric Square-Wave	Constant Current	Square Wave	SOC symmetric Square-Wave
Standalone Estimation	$\frac{\sigma_V}{\alpha\sqrt{N}}$	$\frac{\sigma_V}{\alpha\sqrt{N}}$	$\frac{\sigma_V}{\alpha\sqrt{N}}$	$\frac{\sqrt{3}\sigma_V}{\alpha\sqrt{N}\nabla SOC}$	$\frac{2\sqrt{3}\sigma_V}{\alpha\sqrt{N}\nabla SOC}$	$\frac{4\sqrt{3}\sigma_V}{\alpha\sqrt{N}\nabla SOC}$	$\frac{\sigma_V}{I_0 R\sqrt{N}}$	$\frac{\sigma_V}{I_0 R\sqrt{N}}$	$\frac{\sigma_V}{I_0 R\sqrt{N}}$
Combined 2-state/parameter Estimation SOC/Q	$\frac{2\sigma_V}{\alpha\sqrt{N}}$	$\frac{2\sigma_V}{\alpha\sqrt{N}}$	$\frac{\sigma_V}{\alpha\sqrt{N}}$	$\frac{2\sqrt{3}\sigma_V}{\alpha\sqrt{N}\nabla SOC}$	$\frac{4\sqrt{3}\sigma_V}{\alpha\sqrt{N}\nabla SOC}$	$\frac{4\sqrt{3}\sigma_V}{\alpha\sqrt{N}\nabla SOC}$		\	
SOC/R	∞	$\frac{\sigma_V}{\alpha\sqrt{N}}$	$\frac{\sigma_V}{\alpha\sqrt{N}}$		\		∞	$\frac{\sigma_V}{I_0 R\sqrt{N}}$	$\frac{\sigma_V}{I_0 R\sqrt{N}}$
Q/R		\		$\frac{2\sqrt{3}\sigma_V}{\alpha\sqrt{N}\nabla SOC}$	$\frac{2\sqrt{3}\sigma_V}{\alpha\sqrt{N}\nabla SOC}$	$\frac{4\sqrt{3}\sigma_V}{\alpha\sqrt{N}\nabla SOC}$	$\frac{2\sigma_V}{I_0 R\sqrt{N}}$	$\frac{\sigma_V}{I_0 R\sqrt{N}}$	$\frac{\sigma_V}{I_0 R\sqrt{N}}$
Combined 3-state/parameter Estimation	∞	$\frac{2\sigma_V}{\alpha\sqrt{N}}$	$\frac{\sigma_V}{\alpha\sqrt{N}}$	∞	$\frac{4\sqrt{3}\sigma_V}{\alpha\sqrt{N}\nabla SOC}$	$\frac{4\sqrt{3}\sigma_V}{\alpha\sqrt{N}\nabla SOC}$	∞	$\frac{\sigma_V}{I_0 R\sqrt{N}}$	$\frac{\sigma_V}{I_0 R\sqrt{N}}$

3)   under SOC-symmetric square-wave current

- all three state/parameters can be estimated in group of 2 or 3 with no loss of accuracy.

It is noted that the SOC-symmetric square-wave current is the best current profile among the three for estimation as the accuracy will not degrade for any state/parameter under combined estimation. The SOC-symmetric square-wave also has the same baseline (standalone estimation) accuracy as that under the other two profiles for SOC and resistance. The only exception appears to be the capacity as the error standard deviation is 4 times of that under constant current or twice of that under square wave. The reason is the smaller SOC swing under the SOC-symmetric square-wave given the same current magnitude

I_0. Higher current can be applied to increase the SOC swing and improve the accuracy for capacity estimation.

Simulation has been performed based on the equivalent circuit model of the NMC battery to verify the theoretical derivation. In the simulation, the square-wave current was used, with $I_0 = 10\,A$, $SOC_0 = 10\%$ and a total simulation time of 2700 seconds giving a maximum SOC of 90%. The state and parameters were estimated based on the least squares algorithm using 12 data points ($N = 12$) which were equally distributed in time. Gaussian noise with a standard deviation of 10 mV was added to the voltage signal, and the simulation was repeated by 10000 times. The standard deviation of the estimation errors were calculated over repeated simulation and compared with that predicted by the derived Cramer-Rao bound. The results are summarized in Figure 8–10. In all three figures, subplot (a) shows the
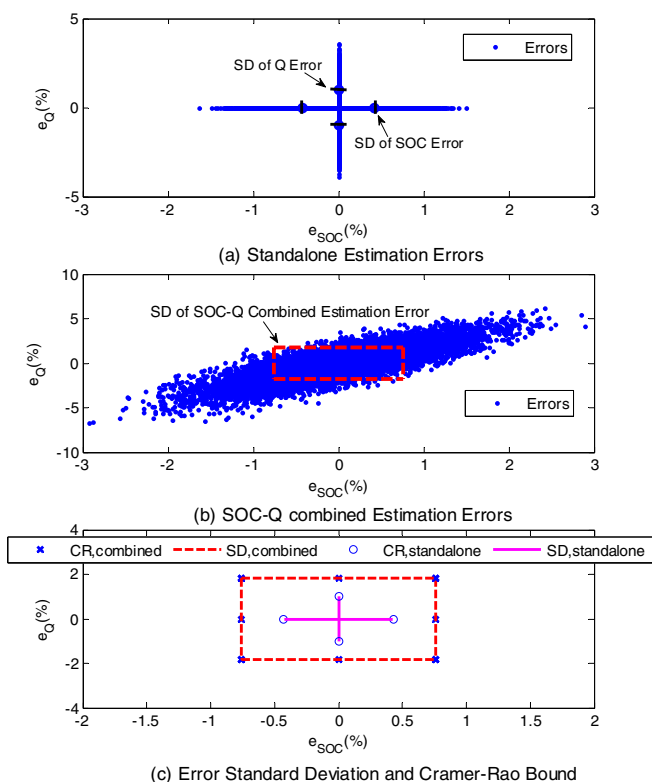

(a) Standalone Estimation Errors

(b) SOC-Q combined Estimation Errors

(c) Error Standard Deviation and Cramer-Rao Bound

Figure 8. SOC and Capacity Estimation Errors under Standalone and Combined Estimation (using square wave current and NMC equivalent circuit model).

(a) Standalone Estimation Errors

(b) SOC-R Combined Estimation Errors

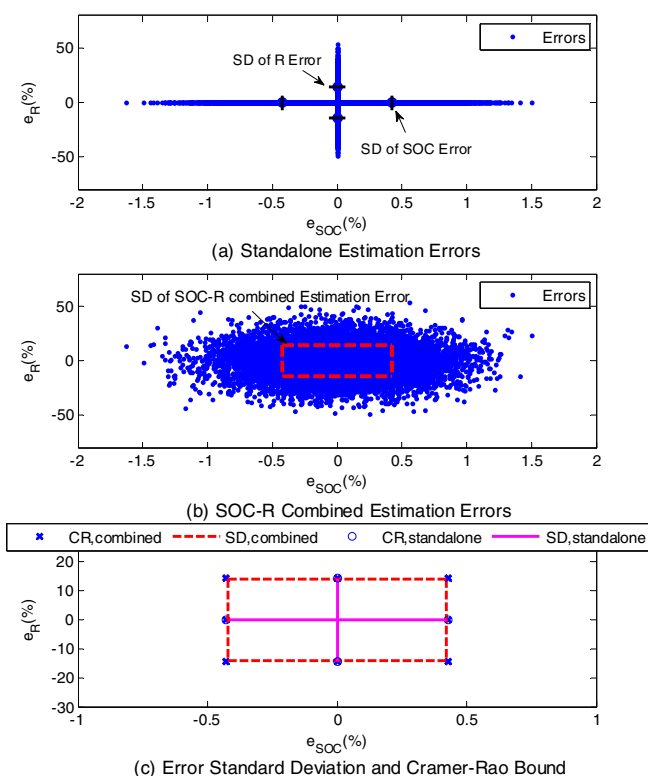(c) Error Standard Deviation and Cramer-Rao Bound

Figure 9. SOC and Resistance Estimation Errors under Standalone and Combined Estimation (using square wave current and NMC equivalent circuit model).

(a) Standalone Estimation Errors

(b) Q-R combined Estimation Errors

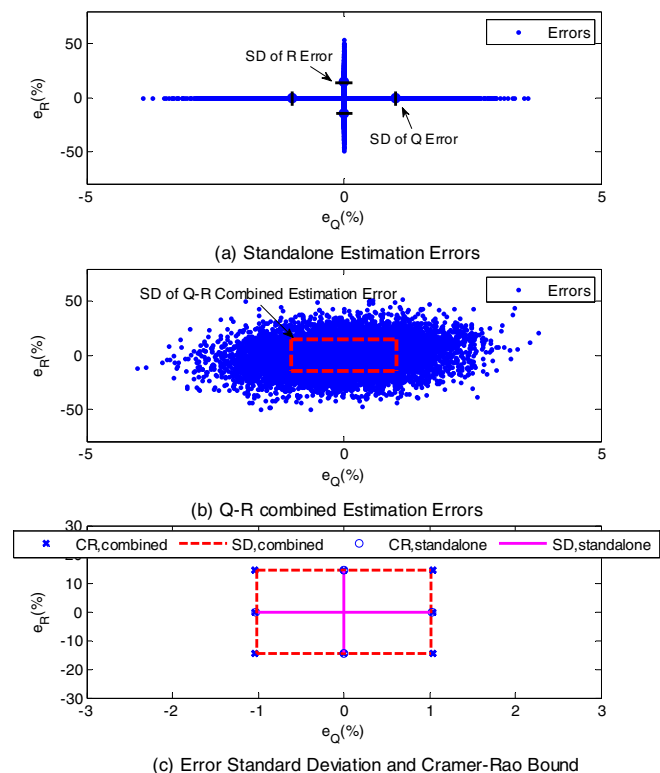(c) Error Standard Deviation and Cramer-Rao Bound

Figure 10. Capacity and Resistance Estimation Errors under Standalone and Combined Estimation (using square wave current and NMC equivalent circuit model).

standalone estimation errors of two state/parameters over the repeated estimation. The errors, denoted by dots, spread over the x and y axis of the e_{SOC}-e_Q plane. Subplot (b) presents the distribution of errors under combined estimation over the e_{SOC}-e_Q plane, and the standard deviation of the estimation errors is labeled by the red dash frame. In subplot (c), the standard deviation of the estimation errors is compared with that predicted by the derived Cramer-Rao bound. It is seen that in all cases, the Cramer-Rao bound matches well with the actual standard deviation, demonstrating the validity of the derivation. The results also agree with the prediction listed in Table III for the square-wave current input. Using the error standard deviation (SD) under standalone estimation as the benchmark, the SOC estimation error SD under combined SOC-Q estimation is twice as much, and the error SD under combined SOC-R estimation remains unchanged. Similarly, the capacity estimation error SD doubles under SOC-Q combined estimation and does not change under Q-R combined estimation. The resistance estimation error SDs are the same in all cases.

Conclusions

The accuracy of battery state/parameter estimation is affected by the characteristics of the battery as well as those of the data set. The main contributing factors to the accuracy of SOC estimation are the slope of the OCV curve and number of data points, while the accuracy of capacity estimation is affected by both OCV slope and SOC variation, and that of resistance estimation depends heavily on the current magnitude. The derived error bounds not only agree with the existing rule of thumb for battery state/parameter estimation, but also quantify the effect of the contributing factors.

When some of the state/parameters are being estimated in a combined fashion, loss of accuracy (as compared to standalone estimation) is usually expected. As an extreme example, under constant current

input, the error variances for SOC and resistance combined estimation are infinity (assuming constant OCV slope), indicating no estimability. Nevertheless, it is still possible to avoid or minimize this loss of accuracy if the current profile satisfies certain patterns. For example, if the current adds up to zero over the data set, e.g. under square-wave current shown in Figure 3c, the combined SOC and R estimation will not only become possible, but also be free from loss of accuracy. In general, if the current profile is designed such that current sequence I_k, SOC variation sequence ΔSOC_k, and the product sequence $I_k \Delta SOC_k$ are all zero-sum over the data set, the combined estimation will not suffer from extra loss of accuracy compared with standalone estimation. Such current pattern will maximize the information contained in the data set for state/parameter estimation, and could be considered as a guideline for experiment design.

The methods and results presented in this paper can be extended in several directions in future work. First, the analytic bounds for other critical battery state/parameters, such as the R-C pairs in the equivalent circuit model, can also be derived by following the same methodology. Second, it is also interesting and of practical use to derive the bounds under other typical current inputs, e.g. the sinusoidal current, and to eventually design a specific current optimizing the identifiability by minimizing the bounds. In addition, the current noise has not been considered in this work at present. It is possible to incorporate the current noise by using the total least squares framework.[31,55]

References

1. P. Ramadass, B. Haran, P. M. Gomadam, R. White, and B. N. Popov, "Development of first principles capacity fade model for Li-ion cells," *Journal of the Electrochemical Society*, **151**(2), A196 (2004).
2. X. Lin, J. Park, L. Liu, Y. Lee, A. M. Sastry, and W. Lu, "A comprehensive capacity fade model and analysis for li-ion batteries," *Journal of The Electrochemical Society*, **160**(10), A1701 (2013).
3. M. Safari, M. Morcrette, A. Teyssot, and C. Delacourt, "Multimodal physics-based aging model for life prediction of Li-ion batteries," *Journal of The Electrochemical Society*, **156**(3), A145 (2009).
4. G. K. Prasad and C. D. Rahn, "Model based identification of aging parameters in lithium ion batteries," *Journal of power sources*, **232**, 79 (2013).
5. M. T. Lawder, P. W. C. Northrop, and V. R. Subramanian, "Model-Based SEI Layer Growth and Capacity Fade Analysis for EV and PHEV Batteries and Drive Cycles," *Journal of The Electrochemical Society*, **161**(14), A2099 (2014).
6. J. R. Belt, D. M. Bernardi, and V. Utgikar, "Development and Use of a Lithium-Metal Reference Electrode in Aging Studies of Lithium-Ion Batteries," *Journal of The Electrochemical Society*, **161**(6), A1116 (2014).
7. L. Lu, X. Han, J. Li, J. Hua, and M. Ouyang, *Journal of Power Sources*, **226**, 272 (2013).
8. X. Lin, A. G. Stefanopoulou, P. Laskowsky, J. S. Freudenberg, Y. Li, and R. D. Anderson, *Proceedings of ASME Dynamic Systems and Control Conference*, p. 393 (2011).
9. Y. Cadirci and Y. Ozkazanc, *Journal of Power Sources*, **129**, 330 (2004).
10. K. Ng, C. Moo, Y. Chen, and Y. Hsieh, *Applied Energy*, **86**, 1506 (2004).
11. M. Dubarry, V. Svoboda, R. Hwu, and B. Y. Liaw, *Journal of Power Sources*, **174**, 1121 (2007).
12. X. Lin, H. E. Perez, S. Mohan, J. B. Siegel, A. G. Stefanopoulou, Y. Ding, and M. P. Castanier, "A lumped-parameter electro-thermal model for cylindrical batteries," *Journal of Power Sources*, **257**, 1 (2014).
13. T. K. Dong, A. Kirchev, F. Mattera, J. Kowal, and Y. Bultel, "Dynamic modeling of Li-ion batteries using an equivalent electrical circuit," *Journal of the Electrochemical Society*, **158**(3), A326 (2011).
14. P. L. Moss, G. Au, E. J. Plichta, and J. P. Zheng, "An electrical circuit for modeling the dynamic response of li-ion polymer batteries," *Journal of The Electrochemical Society*, **155**, 12, A986 (2008).
15. M. W. Verbrugge and R. S. Conell, "Electrochemical and thermal characterization of battery modules commensurate with electric vehicle integration," *Journal of the Electrochemical Society*, **149**(1), A45 (2002).
16. M. Charkhgard and M. Farrokhi, "State-of-charge estimation for lithium-ion batteries using neural networks and EKF," *Industrial Electronics, IEEE Transactions*, **57**(12), 4178 (2010).
17. C. C. Chan, E. W. C. Lo, and Shen Weixiang, "The available capacity computation model based on artificial neural network for lead–acid batteries in electric vehicles," *Journal of Power Sources*, **87**(1), 201 (2000).
18. M. Doyle, T. F. Fuller, and J. Newman, "Modeling of galvanostatic charge and discharge of the lithium/polymer/insertion cell," *Journal of the Electrochemical Society*, **140**(6), 1526 (1993).
19. W. B. Gu and C. Y. Wang, "Thermal-Electrochemical Modeling of Battery Systems," *Journal of The Electrochemical Society*, **147**(8), 2910 (2000).
20. J. C. Forman, S. Bashash, J. L. Stein, and H. K. Fathy, "Reduction of an electrochemistry-based Li-ion battery model via quasi-linearization and Padé approximation," *Journal of the Electrochemical Society*, **158**(2), A93 (2011).

21. D. Di Domenico, A. G. Stefanopoulou, and G. Fiengo, "Lithium-ion battery state of charge and critical surface charge estimation using an electrochemical model-based extended Kalman filter," *Journal of dynamic systems, measurement, and control*, **132**(6), 061302 (2010).

22. K. A. Smith, C. D. Rahn, and C.-Y. Wang. "Control oriented 1D electrochemical model of lithium ion battery," *Energy Conversion and Management*, **48**(9), 2565 (2007).

23. E. Prada, D. Di Domenico, Y. Creff, J. Bernard, V. Sauvant-Moynot, and F. Huet, "Simplified electrochemical and thermal model of LiFePO4-graphite Li-ion batteries for fast charge applications," *Journal of The Electrochemical Society*, **159**(9), A1508 (2012).

24. G. L. Plett, "Extended Kalman filtering for battery management systems of LiPB-based HEV battery packs: Part 3. State and parameter estimation," *Journal of power sources*, **134**(2), 277 (2004).

25. F. Sun, X. Hu, Y. Zou, S. Li, and S. "Adaptive unscented Kalman filtering for state of charge estimation of a lithium-ion battery for electric vehicles," *Energy*, **36**(5), 3531 (2011).

26. Il-S. Kim, "The novel state of charge estimation method for lithium battery using sliding mode observer," *Journal of Power Sources*, **163**(1), 584 (2006).

27. F. Zhang, et al., "Estimation of Battery State of Charge With Observer: Applied to a Robot for Inspecting Power Transmission Lines," *Industrial Electronics, IEEE Transactions*, **59**(2), 1086 (2012).

28. S. J. Moura, M. Krstic, and N. A. Chaturvedi, "Adaptive pde observer for battery soc/soh estimation," *ASME 2012 5th Annual Dynamic Systems and Control Conference joint with the JSME 2012 11th Motion and Vibration Conference*, American Society of Mechanical Engineers (2012).

29. X. Lin, A. G. Stefanopoulou, Y. Li, and R. D. Anderson, "State of charge estimation of cells in series connection by using only the total voltage measurement," in *Proceedings of American Control Conference*, p. 704 (2013)

30. X. Lin, A. G. Stefanopoulou, Y. Li, and R. D. Anderson, "State of Charge Imbalance Estimation for Battery Strings under Reduced Voltage Sensing," *IEEE Transactions on Control Systems Technology*, **23**, 1052 (2015).

31. G. L. Plett, "Recursive approximate weighted total least squares estimation of battery cell total capacity," *Journal of Power Sources*, **196**(4), 2319 (2011).

32. M. Verbrugge and B. Koch, "Generalized recursive algorithm for adaptive multiparameter regression application to lead acid, nickel metal hydride, and lithium-ion batteries," *Journal of The Electrochemical Society*, **153**(1), A187 (2006).

33. Bhaskar Saha, et al., "Prognostics methods for battery health monitoring using a Bayesian framework," *Instrumentation and Measurement, IEEE Transactions*, **58**(2), 291 (2009).

34. Y.-H. Chiang, W.-Y. Sean, and J.-C. Ke, "Online estimation of internal resistance and open-circuit voltage of lithium-ion batteries in electric vehicles," *Journal of Power Sources*, **196**(8), 3921 (2011).

35. E. Wan and A. Nelson, *Kalman Filtering and Neural Networks*, Chapter 5: Dual extended Kalman filter methods. Wiley/Inter-Science (2001).

36. S. Santhanagopalan and R. E. White, "Online estimation of the state of charge of a lithium ion cell," *Journal of Power Sources*, **16**(2), 1346 (2006).

37. S. Lee, J. Kim, J. Lee, and B. Cho, "State-of-charge and capacity estimation of lithium-ion battery using a new open-circuit voltage versus state-of-charge," *Journal of Power Sources*, **185**, 1367 (2008).

38. J. Kim, S. Lee, and B. H. Cho, "Complementary cooperation algorithm based on DEKF combined with pattern recognition for SOC/capacity estimation and SOH prediction," *IEEE Transactions on Power Electronics*, **27**, 436 (2012).

39. M. Rubagotti, S. Onori, and G. Rizzoni, "Automotive battery prognostics using dual extended kalman filter," in *Proceedings of the ASME 2009 Dynamic Systems and Control Conference* (2009).

40. C. Hu, B. D. Youn, and J. Chung, "A multiscale framework with extended kalman filter for lithium-ion battery soc and capacity estimation," *Applied Energy*, **92**, 694 (2012).

41. H. He, R. Xiong, and H. Guo, "Online estimation of model parameters and state-of-charge of lifepo4 batteries in electric vehicles," *Applied Energy*, **89**, 413 (2012).

42. H. Dai, X. Wei, and Z. Sun, "State and parameter estimation of a HEV li-ion battery pack using adaptive Kalman filter with a new soc-ocv concept," in *International Conference on Measuring Technology and Mechatronics Automation* (2009).

43. L. Zhang, C. Lyu, G. Hinds, L. Wang, W. Luo, J. Zheng, and K. Ma, "Parameter Sensitivity Analysis of Cylindrical LiFePO4 Battery Performance Using Multi-Physics Modeling," *Journal of The Electrochemical Society*, **161**(5), A762 (2014).

44. J. Marcicki, F. Todeschini, S. Onori, and M. Canova, "Nonlinear Parameter Estimation for Capacity Fade in Lithium-Ion Cells Based on a Reduced-Order Electrochemical Model", *Proceedings of American Control Conference*, p. 572 (2012).

45. V. Ramadesigan, K. Chen, N. A. Burns, V. Boovaragavan, R. D. Braatz, and V. R. Subramanian, "*Parameter estimation and capacity fade analysis of lithium-ion batteries using reformulated models*", *Journal of The Electrochemical Society*, **158**(9), A1048 (2011).

46. E. L. Lehmann and G. Casella, *Theory of point estimation*, Vol. 31, Springer (1998).

47. A. P. Schmidt, M. Bitzer, Á. W. Imre, and L. Guzzella, "Experimentdriven electrochemical modeling and systematic parameterization for a lithium-ion battery cell," *J. Power Sour.*, **195**(15), 5071 (2010).

48. J. C. Forman, S. J. Moura, J. L. Stein, and H. K. Fathy, "Genetic identification and fisher identifiability analysis of the Doyle–Fuller–Newman model from experimental cycling of a LiFePO4 cell," *Journal of Power Sources*, **210**, 263 (2012).

49. J. Vazquez-Arenas, L. E. Gimenez, M. Fowler, T. Han, and S. K. Chen, "A rapid estimation and sensitivity analysis of parameters describing the behavior of commercial Li-ion batteries including thermal analysis", *Energy Conversion and Management*, vol. **87**, p. 472 (2014).

50. A. Sharma, H. K. Fathy, and H. K. "Fisher identifiability analysis for a periodically-excited equivalent-circui1t lithium-ion battery model", *Proceedings of American Control Conference*, 274 (2014).

51. X. Lin, "Adaptive estimation of thermal dynamics and charge imbalance in battery strings," Ph. D. dissertation, Dept. Mech. Eng., Univ. Michigan, Ann Arbor, MI, USA (2014).

52. M. Rothenberger, J. Anstrom, S. Brennan, and H. K. Fathy, "Maximizing Parameter Identifiability of an Equivalent-Circuit Battery Model using Optimal Periodic Input Shaping", *Proceedings of ASME Dynamic Systems and Control Conference* (2014).

53. H. Cramér, *Mathematical methods of statistics*, Vol. 9, Princeton university press (1999).

54. J. Wang, M. W. Verbrugge, P. Liu, and P. "Composite Titanate–Graphite Negative Electrode for Improved State-of-Charge Estimation of Lithium-Ion Batteries," *Journal of The Electrochemical Society*, **157**(2), A185 (2010).

55. G. H. Golub and C. F. Van Loan, "An analysis of the total least squares problem," *SIAM Journal on Numerical Analysis*, **17**(6), 883 (1980).

56. N. A. Samad, J. B. Siegel, and A. G. Stefanopoulou, "Parameterization and validation of a distributed coupled electro-thermal model for prismatic cells," *ASME 2014 Dynamic Systems and Control Conference*, American Society of Mechanical Engineers (2014).

57. C.-T. Chen, *Linear system theory and design*, Oxford University Press, Inc. (1995).

58. S. M. M. Alavi, A. Mahdi, S. J. Payne, and D. A. Howey, "Structural identifiability of battery equivalent circuit models," arXiv preprint arXiv:1505.00153 (2015).